Calculation of shapes of dipolar domains in insoluble monolayers: Analysis of shape stability and transitions

M. A. Mayer and T. K. Vanderlick[a)]
Department of Chemical Engineering, University of Pennsylvania, Philadelphia, Pennsylvania 19104-6393

(Received 20 December 1993; accepted 16 February 1994)

Dispersed domains in two-phase systems often exhibit complex and intriguing morphologies. For many of these systems, it is possible to predict the shape of such a domain through an evaluation of the free energy. In this paper, we present a numerical technique to calculate domain shapes through a variational approach. This is a significant extension to previous work which has primarily involved examining free energies of specific classes of shapes. The solution diagram is presented in the neighborhood of the first four bifurcations from a circle and the affect of domain size is examined. We find the only stable domain shapes are circular or bilobed. More importantly, we find that the transition between these two shapes is discontinuous, contrary to the findings of previous shape studies. Examining the free energy functional in the neighborhood of stable solutions, we find that, in general, domain shape calculations are best applied to small nonelongated domains. Finally, we present *graphical differentiation*, a numerical technique we developed to enable solution of the problem.

I. INTRODUCTION

Numerous diverse physical systems exhibit fascinating patterns due to internal domain formation. The essence of these patterns may arise from the shape of individual domains, the arrangement of domains, or both. Such systems include ferromagnetic fluids,[1-3] thin magnetic films,[4] superconducters,[5] and phospholipid monolayers residing at the air/water interface.[6-9] While many observed shapes and patterns emerge from growth kinetics, they often evolve into stable conformations which are independent of their history of formation. In recent years, much work has been initiated to predict domain shapes and shape transitions using free energy analyses. All of these attempts have been restricted to one of three approaches: (1) direct comparison of the energies of given shapes;[10-13] (2) variational analysis of the stability of a given shape;[14,15] or (3) tracking shape evolution through a curve dynamics formalism based on a static free energy functional.[1] None of these approaches is expressly designed for (or in the first two cases, capable of) predicting domain shapes which minimize free energy.

In this study, we build on the variational approach to predict the shapes of phospholipid domains. Instead of simply examining the functional derivatives of energy for a given shape, however, we take the next logical step and solve the Euler–Lagrange equation, which is formed by setting the first functional derivative equal to zero. The complexity of this undertaking is by no means conceptual; it is in the implementation. The Euler–Lagrange equation is both nonlinear and integral differential. Moreover, it does not fall into any of the traditional classes of problems common to scientific or engineering work. The closest example of which we are aware is the calculation of the shape of a rotating drop by Brown and Scriven.[16] The free energy functional for the phospholipid domain, however, contains elements which render the problem significantly harder.

The purpose of this paper is twofold. First, we present the results obtained by solving the Euler–Lagrange equation for domain shape, especially those results which could not have been found using any of the three previously applied approaches. Second, we present *graphical differentiation*, the novel numerical tool we developed, necessary for efficient solution of the problem. The remainder of this paper is therefore divided into three main topics. Section II presents the energy model and outlines the general solution strategy (specific implementation details are provided in an appendix). Section III presents and discusses the results of our shape calculations, comparing them when applicable to studies by McConnell,[10] Vanderlick and Möhwald,[12] and Deutch and Low.[15] Section IV presents the method of *graphical differentiation*.

II. BACKGROUND

A. Energy model

Following the analysis of McConnell *et al.*,[10] an isolated domain of fixed area (A_0) takes the shape which minimizes the domain's free energy. Clearly, in such an analysis, only shape dependent contributions to the free energy need be considered. For domains in a phospholipid monolayer, these contributions arise from interfacial tension and electrostatic repulsion.

The interfacial free energy arises from the excess free energy associated with the existence of an interface between the domain and the surrounding continuous phase. It is modeled here as simply a line tension λ acting along the domain perimeter P,

$$F^I = \lambda P. \tag{2.1}$$

a)To whom correspondence should be addressed.

 0021-9606/94/100(11)/8399/9/$6.00

Because F^I scales as the perimeter, this contribution to the free energy promotes compact circular domains.

The electrostatic energy arises from the dipole moment associated with phospholipid molecules at an air/water interface. The shape dependency of this contribution is due to the fact that domains possess higher dipole concentrations than the less dense continuous phase which surrounds them. In this work, the axis of the dipole moment is assumed to be normal to the water surface. The electrostatic free energy F^E is therefore modeled as

$$F^E=\frac{\mu^2}{2}\int_D\int_D \frac{g(|\mathbf{r}-\mathbf{r}'|)}{|\mathbf{r}-\mathbf{r}'|^{-3}}\, d^2\mathbf{r}'\, d^2\mathbf{r}, \tag{2.2}$$

where D is all points in the domain, μ is the difference between the dipole density of the domain and that of the continuous phase, and $g(r)$ is the pair distribution function of dipoles. Because parallel oriented dipoles repel one another, F^E promotes elongated, noncircular domains. We note here that some previous shape studies, notably McConnell and Moy[11] and Langer *et al.*,[1] have used an alternate form of F^E which considers the dipolar domain of a charged capacitor rather than a collection of discrete dipoles.

The pair distribution function $g(r)$ present in Eq. (2.2) is necessary to prevent the inclusion of a nonintegrable singularity at $\mathbf{r}=\mathbf{r}'$. Physically, $g(r)$ must vanish at small separations to account for the nonoverlap of dipoles and must approach unity at large separations, where the density distribution becomes uncorrelated. The simplest expression which meets these criteria is the Heaviside step function

$$g(r)=\mathscr{H}(r-\delta)=\begin{cases}1, & r\geq\delta\\ 0, & r<\delta\end{cases} \tag{2.3}$$

where δ is a parameter representing the distance of closest approach between molecules. The inclusion of a Heaviside function in Eq. (2.2), however, makes evaluation of F^E and its derivatives cumbersome. To simplify the evaluation, an alternate pair distribution function has recently been proposed and used in other shape calculations[14,17,18]

$$\tilde{g}(r)=\frac{r^3}{(\sqrt{r^2+\Delta^2})^3}\,. \tag{2.4}$$

Here Δ is a parameter on the order of the smallest interdipole separation. We have previously demonstrated[13] that for the unique case of circular domains, the value of F^E is independent of the choice of Eq. (2.3) or Eq. (2.4) if Δ is set equal to $2\delta/e$. In this study, as with our earlier paper, the Heaviside pair distribution function will be used exclusively.

B. Solution strategy

Calculation of the shape of a fixed-area (A_0) domain requires determining the shape(s) which minimizes the free energy. This may be accomplished using the following numerical algorithm, which is based on that used by Brown and Scriven[16] for the rotating drop problem. This algorithm is primarily a five step process: identification of the appropriate variables, formulation of the governing equations, solution of the equations, evaluation of a solution's stability, and continuation of the solution through parameter space. We are by no means trying to imply that any of these steps are conceptually challenging; this overview is included simply to familiarize the reader to our approach.

1. Identification of the variables

The problem is cast into dimensionless form by scaling all lengths by the interdipole distance δ and all energies by the quantity $\lambda\delta$. Doing so reveals that the solution depends on only two parameters—the domain area A_0 and the ratio of electrostatic to interfacial forces μ^2/λ, henceforth referred to as the dimensionless dipole strength Γ. The free energy equation is thus expressed as

$$F=F^I+F^E=\int_0^{2\pi}\sqrt{R^2(\theta)+R'^2(\theta)}\,d\theta+\frac{\Gamma}{2}\int_0^{2\pi}\int_0^{R(\theta)}\int_0^{2\pi}\int_0^{R(\theta')}\frac{\mathscr{H}[\sqrt{r^2+r'^2-2rr'\cos(\theta-\theta')}-1]}{\sqrt{r^2+r'^2-2rr'\cos(\theta-\theta')^3}}\,r'r\,dr'\,d\theta'\,dr\,d\theta. \tag{2.5}$$

The problem is next transformed from continuous to discrete by approximating the shape of the domain as a linear combination of trial functions

$$R(\theta)=\sum_{i=1}^{N} a_i\Phi_i(\theta), \tag{2.6}$$

where $\Phi_i(\theta)$ are N predefined trial functions on the interval $\theta\in(0,2\pi)$ and $\mathbf{a}$ is the corresponding vector of N unknown shape coefficients, the variables of interest in the discretized problem.

2. Formulation of the governing equations

In order that a shape minimizes the energy of the domain, it must satisfy the condition that the first functional derivative equals zero. Because of the constant area constraint, however, the method of Lagrange multipliers is applied to form the appropriate energy functional, specifically,

$$\mathscr{G}[R(\theta)]=F^E[R(\theta)]+F^I[R(\theta)]+\gamma\left(\frac{1}{2}\int_0^{2\pi}R^2(\theta)d\theta-A_0\right). \tag{2.7}$$

Here γ is the Lagrange multiplier, an additional variable in the problem. For the continuous problem, the governing equations are

$$\frac{\delta \mathcal{G}}{\delta R(\theta)}=0, \quad \frac{1}{2}\int_0^{2\pi} R^2(\theta)d\theta=A_0, \tag{2.8}$$

a complex set of integral-differential equations. The discretized problem, however, requires $N+1$ governing equations. The first N equations are formed by applying Galerkin weighted residuals to the first functional derivative of $\mathcal{G}$—using the trial functions $\Phi(\theta)$ as the weighting functions. This is completely equivalent to differentiating $\mathcal{G}$ with respect to the shape coefficients. The final equation remains the area constraint

$$\mathcal{R}_i=\int_0^{2\pi} \frac{\delta \mathcal{G}}{\delta R(\theta)}\Phi_i(\theta)d\theta=\frac{\partial \mathcal{G}}{\partial a_i}=0, \quad i\in\{1,2,\ldots,N\},$$
$$\mathcal{R}_{N+1}=A(\mathbf{a})-A_0=\frac{\partial \mathcal{G}}{\partial \gamma}=0. \tag{2.9}$$

3. Solution of the equations

Newton's method is used to iteratively solve this set of nonlinear equations. Given a good enough initial guess, it always converges. It does so quadratically. And it provides all of the information necessary for the evaluation of solution stability. To solve Eq. (2.9), Newton's method takes the form

$$\begin{pmatrix}\mathbf{a}\\ \gamma\end{pmatrix}_{k+1}=\begin{pmatrix}\mathbf{a}\\ \gamma\end{pmatrix}_k-\begin{Bmatrix}\mathcal{J} & (\partial A)/(\partial a)\\ [(\partial A)/(\partial a)]T & 0\end{Bmatrix}_k^{-1}\times\begin{bmatrix}(\partial \mathcal{G})/(\partial a_i)\\ A(\mathbf{a})-A_0\end{bmatrix}_k. \tag{2.10}$$

Here $\mathcal{J}$, not to be confused with the full Jacobian for the problem, represents the matrix of second derivatives of $\mathcal{G}$ with respect to the shape coefficients, i.e.,

$$\mathcal{J}_{ij}=\frac{\partial^2 \mathcal{G}}{\partial a_i \partial a_j}, \quad i,j\in\{1,2,\ldots,N\}. \tag{2.11}$$

4. Evaluation of solution stability

A domain shape must not only satisfy the Euler–Lagrange equation to minimize the free energy, it must also satisfy the condition that any area-preserving perturbation to the domain η increase the free energy, i.e.,

$$\eta^T \mathcal{J} \eta>0, \quad \text{where } \sum_i^N \frac{\partial A}{\partial a_i}\eta_i=0. \tag{2.12}$$

A domain shape which satisfies Eq. (2.9) is stable therefore if the minimum value of $\eta^T \mathcal{J} \eta$ is positive. Evaluation of the minimum value of $\eta^T \mathcal{J} \eta$ is a simple matter of applying Golub's[19] algorithm for determining the extrema of a symmetric matrix subject to side constraints. Specifically, the eigenvalues of the matrix $\mathbf{P}\mathcal{J}\mathbf{P}$ are calculated and examined. Here $\mathbf{P}$ is defined as

$$\mathbf{P}=\mathbf{I}-\mathbf{c}\mathbf{c}^T, \quad \text{where } c_i=\left[\sum_j^N\left(\frac{\partial A}{\partial a_j}\right)^2\right]^{-1}\frac{\partial A}{\partial a_i}. \tag{2.13}$$

The vector $\mathbf{c}$ is always an eigenvector of $\mathbf{P}\mathcal{J}\mathbf{P}$ and the associated eigenvalue is always zero. Because $\mathbf{c}$ blatantly violates the area constraint, however, this eigenvalue is discarded. If the remaining eigenvalues are positive, the solution represents an energy minimum, i.e., a stable solution. If any is negative, the shape is unstable with respect to perturbations along any eigenvector associated with a negative eigenvalue. If any of the eigenvalues is zero, the solution is at either a bifurcation or a turning point.[20]

5. Parameter continuation

Up to this point, the algorithm has been based on a fixed value of Γ. To find the onset of a shape transition, however, it is necessary to evaluate the solution as a function of Γ. The simplest means of accomplishing this is through a so-called zeroth-order continuation. The solution is found for an arbitrary value of Γ, the value of Γ is adjusted, and a new solution is found using the previously found solution as the initial guess. This procedure is repeated until the solution has been mapped over the entire range of interest.

The simple continuation method just described, however, cannot be used near a bifurcation or a turning point in Γ. In the neighborhood of either of these points, the Jacobian becomes nearly singular and Newton's method fails to converge due to numerical round-off error. This complication may be circumvented by introducing a new parameter to the problem specifically for continuation. We found it convenient to use for this continuation parameter I_{zz} the in-plane moment of inertia about the origin normalized to a circle of area A_0,

$$I_{zz}=\frac{\pi}{2A_0^2}\int_0^{2\pi} R^4(\theta)d\theta. \tag{2.14}$$

Admittedly I_{zz} cannot be used to continue along the trivial solution branch of circular domains (shown in the next section), but it can be used along all other solution branches. Moreover, because $I_{zz}>1$ on all noncircular branches, it is an ideal parameter for initiating continuation along them, i.e., when the initial guess is a circle. Incorporation of I_{zz} into Newton's method requires treating Γ as an additional variable rather than as a parameter. To accommodate this new variable, Eq. (2.14) is added as an additional residual equation.

III. RESULTS AND DISCUSSION

The heart of the solution diagram is depicted in Fig. 1. Domain shape, as measured by the I_{zz} moment, is plotted as a function of dimensionless dipole strength with representative solution shapes included alongside the curve. Many features of this curve are readily apparent. Circular domains always solve the Euler–Lagrange equation; they are not, however, always stable solutions. They are stable for small Γ, when line tension dominates, and unstable for large Γ, when electrostatics dominates—as intuition would suggest. The onset of circular instability signals the first of many solution bifurcations from the circular solution branch. The values of the four shown bifurcations are given in Table I and compared with values predicted by Keller *et al.*,[10] Vanderlick and Möhwald,[12] and Deutch and Low;[15] the line tension has

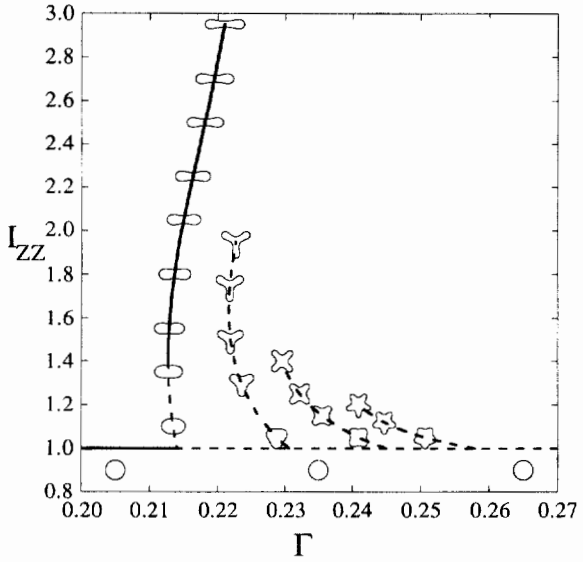

FIG. 1. The solution diagram of domain shape (plotted as normalized I_{zz}) vs dimensionless dipole strength in the neighborhood of the first four bifurcations from a circular domain. Domain area is $10^4\pi\delta^2$. Stable solutions are shown as solid lines; unstable solutions as broken lines. Inset figures depict the shape of the domain at various points along the solution curve.

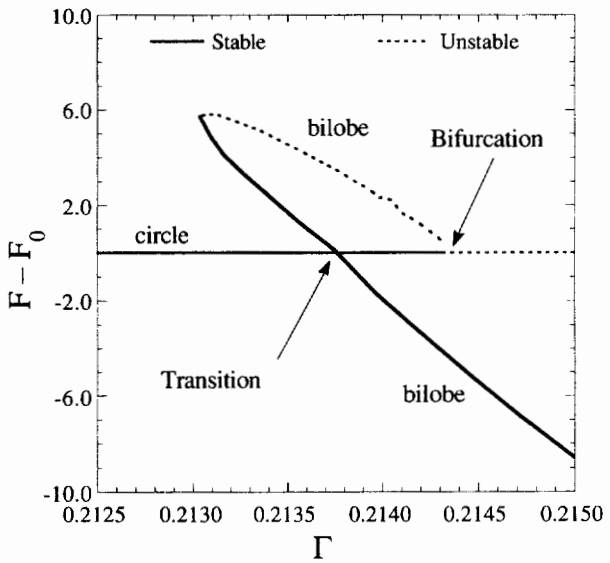

FIG. 2. The free energy difference between circular and bilobed domains in the neighborhood of the first bifurcation. F_0 represents the free energy of a circular domain. Area is $10^4\pi\delta^2$. Stable solutions are shown as solid lines; unstable solutions as broken lines. The formal transition occurs when the circle and bilobe branches cross at $\Gamma=0.2138$.

been adjusted to account for the use of different expressions for F^E in each study.[13] All of these results are in good agreement.

The first solution branch which bifurcates from the circular solution represents "bilobed" domains. The second branch represents "trilobed" domains. Subsequent branches represent increasingly higher order lobed domains. The branches bifurcate subcritically, i.e., I_{zz} initially increases with decreasing Γ. Eventually each branch passes through a turning point, after which I_{zz} increases with increasing Γ. For values of I_{zz} between the bifurcation and the turning point, the solution shapes are unstable with respect to their own class of shapes and all lower order lobed perturbations, e.g., along the trilobed branch, the solutions are unstable to both bilobed and trilobed perturbations. Above the turning point, the solutions are unstable only with respect to lower order lobed perturbations. Assuming that this trend continues for all solution branches, the only noncircular solution branch to ever represent stable shapes is the bilobed branch.

The only shapes which ever minimize the free energy of the phospholipid domain, therefore, are circles at low Γ and bilobes at high Γ. Because the bilobed branch bifurcates subcritically and because the solutions along this branch are unstable up to the turning point, exactly two stable solutions exist when Γ is greater than the turning point value (0.2127) and less than the bifurcation value (0.2143). As shown in Fig. 2, a circular domain initially (reading from low to high Γ) has the lowest free energy; a bilobed domain is metastable. As Γ increases, the free energy of the bilobed domain decreases with respect to the circular domain and eventually becomes the lowest free energy, at which point, circular domains are metastable. Formally, the transition from circles to bilobes as the most stable domain shape occurs when the energies of the two solutions cross ($\Gamma=0.2138$). Both solutions remain, however, local energy minima for the entire range of solution coexistence. An energy barrier must consequently exist between them for the entire range of coexistence. The transition is therefore first order (discontinuous)

TABLE I. A comparison of the onset of circular instability[a] to previous studies: Keller *et al.* (Ref. 10), Vanderlick and Möhwald (Ref. 12), and Deutch and Low (Ref. 15). Previous results were adjusted to correct for the use of different expressions for the electrostatic free energy. Here Γ_n is the value of Γ at the bifurcation to n-lobed domains.

	Reported			Adjusted			
Study	Γ_2	Model used	Correction	Γ_2	Γ_3	Γ_4	Γ_5
Keller *et al.*	0.3762	Capacitor	$\lambda\rightarrow\lambda-2\mu^2$	0.2147			
Vanderlick and Möhwald	0.3764	Capacitor	$\lambda\rightarrow\lambda-2\mu^2$	0.2148	0.2312	0.2456	0.2588
Deutch and Low	0.2734	$\tilde{g}(r)$	$\lambda\rightarrow\lambda-\mu^2$	0.2147	0.2312	0.2456	0.2588
Present Work	0.2143	Heavyside $g(r)$		0.2143	0.2312	0.2455	0.2583

[a]Domain of radius $R=100\,\delta$.

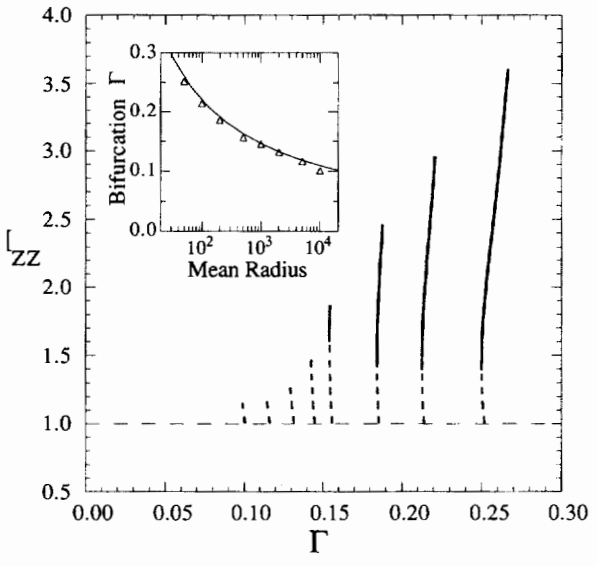

FIG. 3. Bilobe solution branches for various domain sizes, reported as mean radius, $R = \sqrt{A_0/\pi}$. From left to right, the solution curves are for mean radii $10\,000\delta$, 5000δ, 2000δ, 1000δ, 500δ, 200δ, 100δ, and 50δ. The inset graph depicts the bifurcation value of Γ as a function of mean radius—the data points represent each of the shown radii; the solid curve represents the least-squares fit $\Gamma=[4/3+\ln(R/4\delta)]^{-1}$.

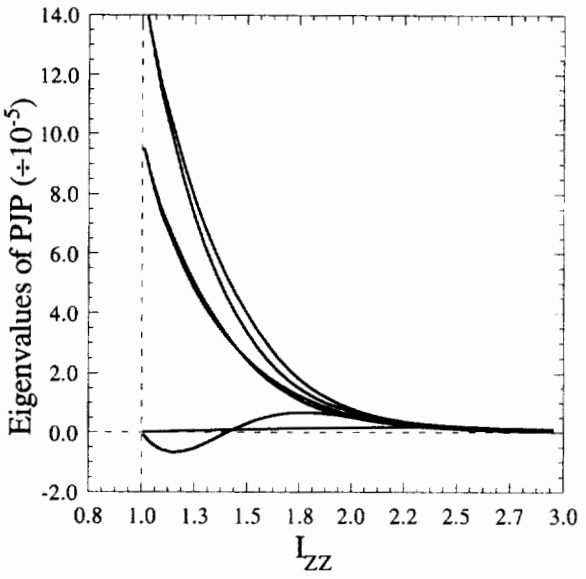

FIG. 4. Lowest six eigenvalues of $\mathbf{P}\mathcal{J}\mathbf{P}$ along the solution curve. The rapid decay along the bilobe branch brings about decreasing ability to predict domain shapes. The eigenvalues exist in pairs due to rotational degeneracy for circular domains—i.e., the limit $l_{zz}=1$.

rather than second order (continuous). One should expect to find experimentally all of the characteristic markings of a first-order transition—notably hysteresis and shape coexistence. Stine and Stratmann[21] have reported results which clearly show shape coexistence in a sterylamine monolayer. Goldstein[22] has observed shape hysteresis in the similar system of ferrofluid domains. No previous domain shape calculation has predicted this behavior.[23]

Figure 3 shows the affect of domain size on the circular to bilobe transition. Specifically, the first solution branch is plotted as in Fig. 1 for various domain areas. By plotting the bifurcation as a function of domain size and fitting a curve through this data, the value of the bifurcation is found to be $\{1.33+\ln[R/(4\delta)]\}^{-1}$. This is exactly the same relationship predicted for the hypothetical circular to elliptical transition.[13] This relationship also follows the experimentally observed trend that small domains are more likely to be circular, while large domains are more likely to be noncircular.

Possibly one of the most important facts about the solution cannot be seen in either Fig. 1 or Fig. 3. The determinant of the Jacobian matrix decays rapidly with increasing l_{zz} or A_0. Physically, the potential well which governs domain shape is becoming shallower; the driving force is becoming weaker, allowing for larger acceptable perturbations. This is witnessed in Fig. 4, which shows the first six eigenvalues for the bilobed branch—a measure of the energy cost associated with shape perturbations along the corresponding eigenvector. The physical loss of driving force is reflected in the numerical calculation of domain shape. With the Jacobian approach being singular, its inversion becomes increasingly sensitive to numerical round-off error; Newton's method eventually fails to converge. The noncircular solution branches shown in Figs. 1 and 3 therefore do not represent the entire branch; they were terminated upon failure to achieve convergence. Although more of the solution branch could have been calculated by taking increasingly smaller continuation steps or using increasingly more accurate quadrature techniques, the return is increasingly small. Doubling the quadrature discretization takes twice as much computation time and only expands the curve from $l_{zz}=2.95$ to 3.25. Halving the step continuation step size also takes twice as much computation time and only expands the curve to $l_{zz}=3.0$. Predictions of domain shapes through energy minimization techniques are best suited for conditions which produce fairly compact, not necessarily circular, domains. Fortunately, these are also the conditions under which the physical driving force is most pronounced.

IV. GRAPHICAL DIFFERENTIATION

Although the solution strategy presented in Sec. II is conceptually straightforward, the actual implementation is hampered by the derivatives of the electrostatic contribution to the free energy. Although the Heaviside function prevents F^E from containing a singularity, it makes numerical integration tedious. The Heaviside function is therefore removed from the definition of F^E through a prudent coordinate transformation. Unfortunately, this change of variables introduces a new complication. The second derivative of F^E cannot be evaluated in the new coordinate system and cannot be transformed back into the original coordinate system. To confront this problem, we could have used finite differencing of the first derivative. This method, however, introduces additional numerical round-off error. Instead, we devised the novel tool, *graphical differentiation*, which enables us to express $(\partial^2 F^E)/(\partial a_i a_j)$ in an evaluable form.

The first step in evaluating the derivatives of F^E is differentiation of Eq. (2.2), yielding the first derivative of F^E with respect to **a**,

$$\frac{\partial F^E}{\partial a_i} = \Gamma \int_0^{2\pi} d\theta\, R(\theta)\Phi_i(\theta) \int_0^{2\pi} d\theta' \int_0^{R(\theta')} \frac{\mathcal{H}[\sqrt{R(\theta)^2+r'^2-2R(\theta)r'\cos(\theta-\theta')}-1]}{\sqrt{R(\theta)^2+r'^2-2R(\theta)r'\cos(\theta-\theta')^3}}\, r'\,dr'. \tag{4.1}$$

Clearly Eq. (4.1) cannot be integrated analytically and numerical integration, although possible, would require extremely fine discretization in the neighborhood of the point **r**, or $[R(\theta),\theta]$. Moreover, differentiation of Eq. (4.1) would spawn a Dirac delta function, the result of which could not be evaluated analytically or numerically.

The very integrand of $(\partial F^E)/(\partial a_i)$ suggests utilizing a coordinate transformation. Rather than keeping the center of mass as the origin, a temporary "local" origin is defined at **r** for integration over r' and θ'. Local polar coordinates (ξ,ϕ) replace global polar coordinates (r',θ'); angle $\phi=0$ is defined to point directly away from the global origin (see Fig. 5). Applying this transformation to Eq. (4.1) yields

$$\frac{\partial F^E}{\partial a_i} = \Gamma \int_0^{2\pi} d\theta\, R(\theta)\Phi_i(\theta) \int_0^{2\pi} d\phi \int_0^{\rho(\phi;\theta)} \frac{\mathcal{H}[\xi-1]}{\xi^3}\, \xi\, d\xi. \tag{4.2}$$

Here $\rho(\phi;\theta)$ is the distance between the local origin and the domain boundary at angle ϕ—analogous to $R(\theta)$ for the global origin. In this form, the innermost integral of $(\partial F^E)/(\partial a_i)$ can be evaluated analytically

$$\frac{\partial F^E}{\partial a_i} = \Gamma \int_0^{2\pi} d\theta\, R(\theta)\Phi_i(\theta) \int_{\phi_1(\theta)}^{\phi_2(\theta)} \frac{\rho(\phi;\theta)-1}{\rho(\phi;\theta)}\, d\phi. \tag{4.3}$$

Here $\phi_1(\theta)$ and $\phi_2(\theta)$ are the two angles at which $\rho(\phi;\theta)=1$ (see Fig. 5). Although $(\partial F^E)/(\partial a_i)$ must still be evaluated numerically, it is a significantly simpler integration than that posed by Eq. (4.1). More importantly, the troublesome Heaviside function has been eliminated.

The second derivatives of F^E with respect to **a** are found by differentiation of Eq. (4.3)

$$\frac{\partial^2 F^E}{\partial a_i \partial a_j} = \Gamma \int_0^{2\pi} d\theta\, \Phi_i(\theta) \left[\Phi_j(\theta) \int_{\phi_1(\theta)}^{\phi_2(\theta)} \frac{\rho(\phi;\theta)-1}{\rho(\phi;\theta)}\, d\phi + R(\theta) \int_{\phi_1(\theta)}^{\phi_2(\theta)} \frac{1}{\rho^2(\phi;\theta)} \frac{\partial \rho(\phi;\theta)}{\partial a_j}\, d\phi \right]. \tag{4.4}$$

Evaluation of Eq. (4.4) requires the evaluation of $[\partial\rho(\phi;\theta)]/(\partial a_j)$. Although $\rho(\phi;\theta)$ is well defined, it cannot be expressed in closed form. It can only be determined implicitly through the law of cosines

$$\rho = \sqrt{R^2(\theta)+R^2(\theta')-2R(\theta)R(\theta')\cos(\theta-\theta')}, \tag{4.5}$$

$$\phi = \cos^{-1}\left[\frac{R(\theta')\cos(\theta-\theta')-R(\theta)}{\sqrt{R^2(\theta)+R^2(\theta')-2R(\theta)R(\theta')\cos(\theta-\theta')}} \right].$$

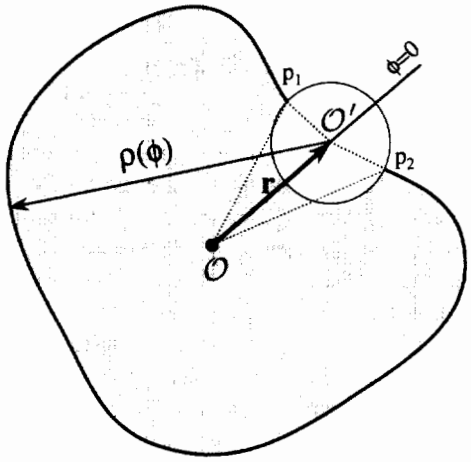

FIG. 5. Coordinate transformation from the global origin ($\mathcal{O}$) to a local origin ($\mathcal{O}'$) located at **r**. The function $\rho(\phi;\theta)$ describes the shape of the domain based on this local origin. The points p_1 and p_2 represent the limits of integration, or where $\rho(\phi;\theta)=1$.

Because $\rho(\phi;\theta)$ cannot be explicitly expressed as a function of **a**, standard differentiation techniques are ineffective in evaluating $[\partial\rho(\phi)]/(\partial a_i)$. We therefore devised the technique *graphical differentiation*.

Graphical differentiation is a geometric approach to a specific problem of differential calculus. Specifically, it examines finite changes in the distance between two points on the domain boundary as the shape of the domain is varied by a finite amount, extrapolating the ratio of these changes to the infinitesimal limit. For the following discussion, the following nomenclature will be used. Point $\mathcal{O}$, as shown in Fig. 6, represents the global origin while point $\mathcal{O}'$ the local origin. The line segment connecting $\mathcal{O}$ and $\mathcal{O}'$ has length l_1 equal to $R(\theta)$. Point $\mathcal{P}$ is the intersection of the line drawn through $\mathcal{O}'$ at angle ϕ with the perimeter of the domain. The line segment connecting $\mathcal{O}$ and $\mathcal{P}$ has length l_2 equal to $R(\theta')$. The line segment connecting $\mathcal{O}'$ and $\mathcal{P}$ has length l_3, equal to $\rho(\phi;\theta)$. Finally, line τ is the tangent to the domain at $\mathcal{P}$ and the β is the angle between τ and $\mathcal{O}\mathcal{P}$.

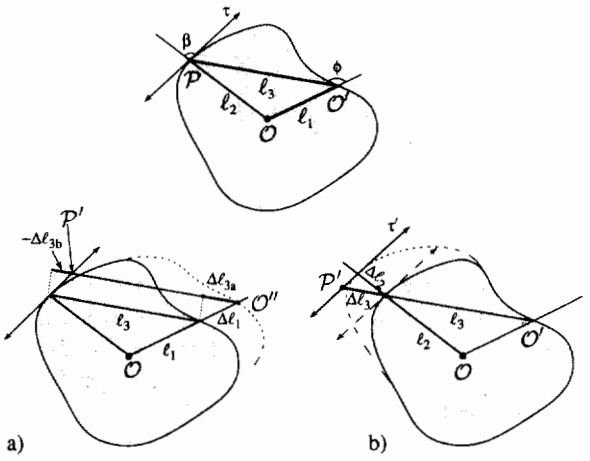

FIG. 6. Graphical differentiation of $\rho(\phi;\theta)$ through finite perturbations of domain shape. The points $\mathscr{O}$ and $\mathscr{O}'$ represent the global and local origins; the line segments l_1, l_2, and l_3 represent $R(\theta)$, $R(\theta')$, and $\rho(\phi;\theta)$, respectively; the point $\mathscr{P}$ represents the point at which $\rho(\phi;\theta)$ intersects the domain perimeter, and β is the angle of the tangent τ at $\mathscr{P}$. (a) When l_1 is increased by Δl_1, the length of l_3 increases at both ends; by Δl_{3a} near the local origin and by Δl_{3b}—shown here as a decrease—near $\mathscr{P}$. (b) When l_2 is increased by Δl_2, the length of l_3 increases by Δl_3.

In this graphical context, the desired derivative $[\partial\rho(\phi;\theta)]/(\partial a_j)$ becomes $(\partial l_3)/(\partial a_j)$. The value of l_3 depends only on the location of the points $\mathscr{O}'$ and $\mathscr{P}$, which in turn depend only on l_1 and l_2. It follows therefore that

$$\frac{\partial l_3}{\partial a_j}=\frac{\partial l_3}{\partial l_1}\frac{\partial l_1}{\partial a_j}+\frac{\partial l_3}{\partial l_2}\frac{\partial l_2}{\partial a_j}$$
$$=\lim_{\Delta l_1\to 0}\frac{\Delta l_3}{\Delta l_1}\Phi_j(\theta)+\lim_{\Delta l_2\to 0}\frac{\Delta l_3}{\Delta l_2}\Phi_j(\theta'). \tag{4.6}$$

The key to graphical differentiation is setting up the problem such that the ratios $(\Delta l_3)/(\Delta l_1)$ and $(\Delta l_3)/(\Delta l_2)$ are independent of Δl_1 and Δl_2 and therefore need not actually be evaluated in the infinitesimal limit. To do so, the perimeter of the domain is approximated by the tangent τ in the neighborhood of $\mathscr{P}$. The ratio $(\Delta l_3)/(\Delta l_1)$ [or $(\Delta l_3)/(\Delta l_2)$] is then determined by extending l_1 by a finite Δl_1 (or l_2 by a finite Δl_2) and evaluating Δl_3. By using the tangent rather than the actual perimeter, the ratios are independent of Δl_1 and Δl_2, while the perimeter is represented correctly in the infinitesimal limit for any linear term.

Before extending either l_1 or l_2, however, the relationship between ϕ and θ' must first be established. In the global origin basis, ϕ is a function of the angles θ and θ' and the shape coefficients **a**. In the local origin basis, θ' is a function of θ, ϕ, and **a**. Because Eq. (4.4) is in the local origin basis, θ and ϕ must be held constant during differentiation. It is θ' which varies, therefore, as the shape of the domain changes.

In Fig. 6(a), the change in l_3 is shown for an increase in l_1 of Δl_1. The point $\mathscr{O}''$ represents the new location of the local origin Δl_1 past $\mathscr{O}'$ on the line $\mathscr{O}\mathscr{O}'$. The point $\mathscr{P}'$ resides at the intersection of the line drawn through $\mathscr{O}''$ at angle ϕ and the tangent τ. Projection of the line segment connecting $\mathscr{O}'$ with $\mathscr{P}$ onto the line segment connecting $\mathscr{O}''$ with $\mathscr{P}'$ reveals two contributions to the change in l_3. These individual changes Δl_{3a} and Δl_{3b} can easily be shown to be

$$\Delta l_{3a}=\Delta l_1\cos(\pi-\phi),$$
$$\Delta l_{3b}=-\Delta l_1\sin(\pi-\phi)\cot(\beta-\phi+\theta'-\theta). \tag{4.7}$$

In Fig. 6(b), the change in l_3 is shown for an increase in l_2 of Δl_2. The local origin remains at $\mathscr{O}'$. The tangent line, however, moves to τ', parallel to τ and separated by the distance Δl_2 along the line $\mathscr{O}\mathscr{P}$. The point $\mathscr{P}'$ resides at the intersection of τ' and the line drawn through $\mathscr{O}'$ at angle ϕ. The change in l_3 is the distance between $\mathscr{P}$ and $\mathscr{P}'$. This change Δl_3 determined from the law of sines is

$$\Delta l_3=\Delta l_2\frac{\sin(\pi-\beta)}{\sin(\beta-\phi+\theta'-\theta)}. \tag{4.8}$$

Plugging Eqs. (4.6)–(4.8) and the definition of $\beta=\cos^{-1}\{[R(\theta)'(\theta')]/[R^2(\theta')+R'^2(\theta')]\}$ into Eq. (4.4) yields

$$\frac{\partial^2 F^E}{\partial a_i\partial a_j}=\Gamma\int_0^{2\pi}d\theta\,\Phi_i(\theta)\left\{\Phi_j(\theta)\int_{\phi_1(\theta)}^{\phi_2(\theta)}\frac{\rho(\phi;\theta)-1}{\rho(\phi;\theta)}\,d\phi\right.$$
$$\left.+R(\theta)\int_{\phi_1(\theta)}^{\phi_2(\theta)}\frac{R(\theta')\Phi_j(\theta')-[R(\theta')\cos(\theta'-\theta)+R'(\theta')\sin(\theta'-\theta)]\Phi_j(\theta)}{\rho^2(\phi)[R(\theta')\cos(\phi-\theta'+\theta)-R'(\theta')\sin(\phi-\theta'+\theta)]}\,d\phi\right\}. \tag{4.9}$$

Through a generous dose of algebra and trigonometric identities, $(d\phi)/(d\theta')$ can be shown to be

$$\frac{d\phi}{d\theta'}=\frac{R(\theta')\cos(\phi-\theta'+\theta)-R'(\theta')\sin(\phi-\theta'+\theta)}{\sqrt{R^2(\theta)+R^2(\theta')-2R(\theta)R(\theta')\cos(\theta'-\theta)}}, \tag{4.10}$$

which allows Eq. (4.9) to be translated cleanly into the global coordinates as

$$\frac{\partial^2 F^E}{\partial a_i \partial a_j} = \Gamma \int_0^{2\pi} d\theta\, \Phi_i(\theta) \left\{ \Phi_j(\theta) \int_{\phi_1(\theta)}^{\phi_2(\theta)} \frac{\rho(\phi;\theta)-1}{\rho(\phi;\theta)}\, d\phi \right.$$

$$\left. + R(\theta) \int_{\theta_1'(\theta)}^{\theta_2'(\theta)} \frac{R(\theta')\Phi_j(\theta') - [R(\theta')\cos(\theta'-\theta) + R'(\theta')\sin(\theta'-\theta)]\Phi_j(\theta)}{\sqrt{R^2(\theta)+R^2(\theta')-2R(\theta)R(\theta')\cos(\theta'-\theta)^3}}\, d\theta' \right\}. \tag{4.11}$$

V. CONCLUSIONS

Direct numerical computation of domain shapes through variational analysis provides information about domains shapes which cannot be acquired using simpler techniques. Where it does overlap previous studies, specifically determination of the onset of circular instability, it produces very comparable results. Numerical computation, however, reveals that the only stable domain shapes are circles and bilobes. Moreover, the transition between these two shapes is discontinuous, a finding backed by experimental data. Finally, examination of solution stability reveals a second, possibly more important, result: the driving force which determines domain shape rapidly decays with increasing domain size and elongation.

The primary obstacle to implementing a numerical calculation of domain shape is evaluation of the derivatives of electrostatic energy. The source of the difficulty, the Heaviside function, can be eliminated through a prudent coordinate transformation. This transformation, however, produces terms which cannot be evaluated directly. Instead, our novel mathematical tool *graphical differentiation* must be employed. Together, the coordinate transformation and *graphical differentiation* completely eliminate this only substantial obstacle.

Future work in domain shape calculation should consist of a two-pronged attack. First, the results presented here should be expanded to examine the effects of tilted dipole moments, anisotropic line tension, and multiple domain interactions. Second, shapes which do not minimize domain free energy should be examined. Such studies might involve dynamic studies similar to those undertaken by Langer *et al.*[1] which find a plethora of metastable domain shapes, and which should not be limited to nearly circular domain shapes as are energy minimizing calculations.

ACKNOWLEDGMENTS

We gratefully acknowledge the support of the donors of the Petroleum Research Fund, administered by the American Chemical Society, the support of the National Science Foundation, through a Presidential Young Investigator Award (CTS-89-57051) to T. K. V. and a Procter and Gamble Fellowship to M. A. M., and the support of Digital Equipment Corporation through a credit allowing for the purchase of a DECStation 5000 upon which the bulk of the above work was accomplished.

APPENDIX: COMPUTER IMPLEMENTATION

Throughout the body of the paper, the solution strategy was presented without specific details. The trial functions and quadrature techniques used to calculate the results given in Sec. III were intentionally absent. An accurate solution diagram must be independent of these details. Careful implementation of numerical methods can, however, significantly improve computation time.

The shape of the domain $R(\theta)$ was approximated using 57 cubic Hermitian basis functions[24] defined over 29 discretization nodes. This is the simplest set of polynomial finite elements which provide both continuous first and second derivatives of $R(\theta)$, both of which are necessary in evaluating the Jacobian. Following conventional usage, two Hermitian polynomials were defined for each discretization node—one with unit magnitude and zero slope; the other with unit slope and zero magnitude. These basis functions, however, as with almost any other choice, allow for translational and rotational degeneracy in the domain shape. Elimination of rotation was accomplished by simply setting the coefficient of the first slope Hermitian polynomial to zero, thus the use of an odd number of basis functions. Elimination of translation was accomplished by imposing two new side constraints on the problem; the x and the y components of the center of mass are set equal zero.

Adaptive discretization[25–27] was used to increase the accuracy of the approximated solution without sacrificing computational efficiency (i.e., without increasing the number of basis functions). Rather than defining discretization nodes at equal intervals of θ, the nodes were distributed such that the domain perimeter was equally partitioned between nodes, i.e.,

$$\mathscr{P}_i = \int_{\theta_i}^{\theta_{i+1}} \sqrt{R^2(\theta)+R'^2(\theta)}\, d\theta - K = 0,$$

$$i \in \{1,2,\ldots,n\}, \tag{A1}$$

where K is the length of perimeter associated with each element and n is the number of nodes $[=\frac{1}{2}(N+1)]$. More basis functions were therefore used in regions where the shape changed the most rapidly. (See Russel *et al.*[26] for a summary of 15 alternative adaptive strategies.) This perimeter adaptive scheme has two attractive qualities: it is conceptually straightforward and it is not susceptible to nodal bifurcations, which may switch the sequence of adjacent nodes.

The nodal positions were solved using a second Newton iteration between each continuation step, as suggested by Benner *et al.*[27] Because the new nodal positions were not solved concurrently with domain shape, the continuation steps had to be small enough that the final shape was not be significantly different from the initial guess. Changing the distribution of the nodes without updating the shape coefficients, however, results in distortion of the initial guess. This

distortion can become large enough that Newton's method fails to converge, even if no continuation step is taken. To minimize distortion, the shape coefficients were recalculated along with the nodal positions such that the square of the difference Λ between the new shape and the original shape was minimized

$$\Lambda=\int_0^{2\pi}[R(\theta)-R^*(\theta)]^2 d\theta. \tag{A2}$$

Here $R(\theta)$ is the shape based on the new coefficients and nodal placement and $R^*(\theta)$ is the shape based on the old coefficients and nodal placement.

All of the many numerical integrations can be grouped into one of two classes: integration over θ or integration over θ'. Because $\rho(\phi;\theta)$ cannot be expressed in closed form, the terms in Eqs. (4.3) and (4.11) integrated over ϕ are actually evaluated over θ'. Integrals over θ have integrands of fairly constant magnitude. They were evaluated using a four-point Gaussian quadrature on each discretization element. Integrals over θ', which descend from F^E, have integrands which vary by many orders of magnitude. Remember that these integrals would have contained a singularity were the pair distribution function absent from the definition of F^E. They were evaluated using a nonuniformly discretized trapezoid rule, specifically,

$$\theta_i'=\theta_1'+(\theta_2'-\theta_1')\,\frac{1+\tanh\{[(2i)/N_\chi]\chi-\chi\}}{2\,\tanh(\chi)}, \tag{A3}$$

For the work presented here, values of $\chi=3$ and $N_\chi=200$ were used. (Note that if $\theta_2'<\theta_1'$, then $2\pi+\theta_2'$ should be substituted for θ_2'.)

[1] S. A. Langer, R. E. Goldstein, and D. P. Jackson, Phys. Rev. A **46**, 4894 (1992).
[2] A. J. Dickstein, S. Erramilli, R. E. Goldstein, D. P. Jackson, and S. A. Langer, Science **261**, 1012 (1993).
[3] R. E. Rosenweig, *Ferrohydrodynamics* (Cambridge University, Cambridge, 1982), Chap. 7.
[4] T. Garel and S. Doniach, Phys. Rev. B **26**, 325 (1982).
[5] L. D. Landau, Zh. Eksp. Theor. Fiz. **7**, 371 (1937).
[6] M. Flörsheimer and H. Möhwald, Chem. Phys. Lipids **49**, 231 (1989).
[7] V. Tscharner and H. M. McConnell, Biophys. J. **36**, 409 (1981).
[8] C. M. Knobler, Science **249**, 870 (1990).
[9] M. Seul, Phys. Status Solidi A **168**, 198 (1990).
[10] D. J. Keller, J. P. Korb, and H. M. McConnell, J. Phys. Chem. **91**, 6417 (1987).
[11] H. M. McConnell and V. T. Moy, J. Phys. Chem. **92**, 4520 (1988).
[12] T. K. Vanderlick and H. Möhwald, J. Phys. Chem. **94**, 886 (1990).
[13] M. A. Mayer and T. K. Vanderlick, Langmuir **8**, 3131 (1992).
[14] H. M. McConnell, J. Phys. Chem. **94**, 4728 (1990).
[15] J. M. Deutch and F. E. Low, J. Phys. Chem. **96**, 7097 (1992).
[16] R. A. Brown and L. E. Scriven, Philos. Trans. R. Soc. London **297**, 5 (1980).
[17] H. M. McConnell, Annu. Rev. Phys. Chem. **42**, 171 (1991).
[18] H. M. McConnell and R. deKoker, J. Phys. Chem. **96**, 7101 (1992).
[19] G. H. Golub, SIAM Rev. **15**, 318 (1973).
[20] M. Kubiček and M. Marek, *Computational Methods in Bifurcation Theory and Dissipative Structures* (Springer, New York, 1983).
[21] K. J. Stine and D. T. Stratmann, Langmuir **8**, 2509 (1992).
[22] R. Goldstein (personal correspondence).
[23] This statement was true at the time of submission. Since then, however, H. M. McConnell and R. deKoker have shown in J. Phys. Chem. **97**, 13419 (1993) that the transition is first order for domains whose shapes are restricted to ovals of Cassini.
[24] G. Strang and G. J. Fix, *An Analysis of the Finite Element Method* (Prentice–Hall, Englewood Cliffs, NJ, 1973).
[25] V. Pereyra and E. G. Sewell, Num. Math. **23**, (1975).
[26] R. D. Russell and J. Christiansen, SIAM J. Num. Anal. **15**, 59 (1978).
[27] R. E. Benner, Jr., H. T. Davis, and L. E. Scriven, SIAM J. Sci. Stat. Comput. **8**, 529 (1987).